1   **Speciated Atmospheric Mercury during Haze and Non-haze Days in**

2   **an Inland City in China**

3

4

5   Qianqian Hong[1,3], Zhouqing Xie[1,2,3*], Cheng Liu[1,2,3*], Feiyue Wang[4], Pinhua Xie[2,3],

6   Hui Kang[1], Jin Xu[2], Jiancheng Wang[1], Fengcheng Wu[2], Pengzhen He[1], Fusheng Mou[2],

7   Shidong Fan[1], Yunsheng Dong[2], Haicong Zhan[1], Xiawei Yu[1], Xiyuan Chi[1], Jianguo

8   Liu[2]

9

10

11   1. School of Earth and Space Sciences, University of Science and Technology of

12   China, Hefei, 230026, China

13   2. CAS Center for Excellence in Regional Atmospheric Environment & Institute of

14   Urban Environment of CAS, Xiamen, 361021, China

15   3. Key Lab of Environmental Optics and Technology, Anhui Institute of Optics and

16   Fine Mechanics, Chinese Academy of Sciences, Hefei, 230031, China

17   4. Centre for Earth Observation Science, and Department of Environment and

18   Geography, University of Manitoba, Winnipeg, MB R3T 2N2, Canada

19

20

21   Correspondence author:

22   zqxie@ustc.edu.cn (Z.Q.X.); chliu81@ustc.edu.cn (C.L.)

23

24

Abstract. Long-term continuous measurements of speciated atmospheric mercury were conducted from July 2013 to June 2014 at Hefei, a mid-latitude inland city in east central China that experiences frequent haze pollution. The mean concentrations ($\pm$ standard deviation) of gaseous elemental mercury (GEM), gaseous oxidized mercury (GOM) and particle-bound mercury (PBM) were 3.95 ± 1.93 ng m^{-3}, 2.49 ± 2.41 pg m^{-3} and 23.3 ± 90.8 pg m^{-3}, respectively, during non-haze days, and 4.74 ± 1.62 ng m^{-3}, 4.32 ± 8.36 pg m^{-3} and 60.2 ± 131.4 pg m^{-3}, respectively, during haze days. Potential source contribution function (PSCF) analysis suggested that the atmospheric mercury pollution during haze days was caused primarily by local mercury emissions, instead of via long-range mercury transport. The disadvantageous diffusion during haze days also favoured the accumulation of atmospheric mercury. Compared to GEM and GOM, PBM was found to be more sensitive to haze pollution. The mean PBM concentration during haze days was 2.5 times that during non-haze days due to elevated concentrations of particulate matter. A remarkable seasonal trend in PBM was also observed with concentration decreasing in the following order in response to the frequency of haze days: autumn, winter, spring and summer. For both non-haze and haze days, GOM concentrations remained at relatively constant during night, but increased rapidly prior to sunrise. This GOM diurnal variation could be due to diurnal variation in air exchange between the boundary layer and free troposphere, but the contribution from photochemical oxidation could not be ruled out. This is supported by simple box-model calculations, which showed that oxidation of GEM to GOM does occur and that the transport of free troposphere GOM alone is not large enough to account for the observed increase in GOM. Our results postulate that NO_2

aggregation with the HgOH intermediate may be a potential mechanism for the enhanced production of GOM during daytime.

1. Introduction

Mercury (Hg) is an environmental pollutant that has received much global attention because of its toxicity and bioaccumulation via the aquatic food chain. The most important transport pathway of mercury is via the atmosphere (Schroeder and Munthe, 1998;Lindqvist and Rodhe, 1985). Operationally, atmospheric mercury is commonly differentiated into three forms: gaseous elemental mercury (GEM), gaseous oxidized mercury (GOM) and particle-bound mercury (PBM). The sum of these three atmospheric speciated mercury is defined as total atmospheric mercury (TAM = GEM + GOM + PBM), and the sum of GEM and GOM is known as total gaseous mercury (TGM = GEM + GOM) (Gustin and Jaffe, 2010;Gustin et al., 2015). GEM is regarded as the dominant form of atmospheric mercury, accounting for over 95% of the total. GEM is stable in the troposphere with a long residence time (0.5–2 yr) and can be transported at the regional to global scale (Schroeder and Munthe, 1998;Lindberg et al., 2007). GEM can be oxidized to GOM through photochemical processes, and further transformed to PBM on aerosol surfaces. GOM and PBM can be readily removed form the air by wet and dry deposition as a result of their high surface affinity and water solubility (Lindqvist and Rodhe, 1985). Thus, the chemical transformation between GEM, GOM and PBM will directly influence the atmospheric lifetime of mercury.

As a result of the rapid industrial development and economic growth of recent decades, China has become one of the major contributors to anthropogenic mercury

emissions to the environment (Wu et al., 2006;Pacyna et al., 2006;Pacyna et al., 2010;Zhang et al., 2015b). Atmospheric mercury emissions from anthropogenic sources in China have been estimated to be in the range of 500-700 tons/yr, accounting for 25-30% of the total global anthropogenic mercury emissions (Streets et al., 2005;Wu et al., 2006). Research into atmospheric mercury in China is therefore critical to the understanding of mercury cycling at both regional and global scales. Long-term observation of atmospheric mercury has been conducted in different regions in China, including both urban and remote areas. TGM concentrations observed in urban and industrial regions of China were in the range of 2.7–35 ng m^{-3}, higher than the values reported for North America and Europe, and for the adjacent Asian countries such as Korea and Japan (Weigelt et al., 2013;Fang et al., 2009;Marumoto et al., 2015). TGM and PBM concentrations in remote areas of China were also found to be higher than those observed in North America and Europe (Fu et al., 2008a;Fu et al., 2008b;Fu et al., 2012;Liu et al., 2010).

In recent years, haze pollution has become a major concern in China due to its impacts on visibility, air quality, and climate. It is well known that haze formation is mainly dependent on the atmospheric relative humidity (RH) and the concentration of airborne particles (Chen et al., 2003;Sun et al., 2013). Most studies on haze have focused on the measurements of airborne particulate matter; few examined the influence of haze on the chemistry of atmospheric mercury, especially PBM. In this study, we conducted one year synchronous observations of speciated atmospheric mercury in Hefei, an inland city of China, which experiences frequent haze events. The comparision of atmospheric mercury under haze days and non-haze days during

95   the study period allows us to examine the formation and deposition mechanisms of

96   mercury, as well as their temporal variations.

97

98   **2.   Methods**

99   **2.1 Study site**

100   Continuous measurements of speciated atmospheric mercury were undertaken in

101   Hefei (31°52′ N, 117°17′ E) from July 2013 to June 2014. Hefei, the capital of Anhui

102   Province, is located in east central China, between the Changjiang (Yangtze River) and

103   the Huaihe (Huai River). Hefei has a humid subtropical climate with four distinct

104   seasons: June-August is considered summer, September-November autumn,

105   December-February winter and March-May spring. The prevailing wind is

106   southeasterly in summer and northwesterly in winter. Like many Chinese cities, Hefei

107   has experienced rapid growth in the past 20 years. The total permanent population is

108   about 7.7 million. The city has also been witnessing an increasing frequency in haze

109   pollution, especially in winter months.

110   The monitoring site was located on the Science Island, a small peninsula on the

111   Dongpu Reservoir in the northwestern outskirts of Hefei (Fig. 1). The sampling and

112   analytical instruments were installed 1.5 m above the rooftop (~ 20 m above the

113   ground) of the main building of Anhui Institute of Optics and Fine Mechanics. Further

114   information about the monitoring site can be found in a previous study (Hu et al.,

115   2014). We chose this area as the monitoring site because it is one of the cleanest areas

116   in Hefei, not adjacent to any direct pollution sources such as power plants, iron and

117   steel works.

118

2.2 Measurements of speciated atmospheric mercury

From July 2013 to June 2014, simultaneous measurements of speciated atmospheric mercury concentrations were performed by an automated Tekran^{TM} mercury speciation system. The system consisted of a Model 2537B mercury analyzer combined with a Model 1130 GOM unit and a Model 1135 PBM unit. The system was configured to measure GEM every 5 min., and GOM and PBM every 2 h.

The details about the Tekran-based mercury speciation system can be found in Landis et al. (2002). In general, the automated measurement process can be summarized as sample collection, thermal desorption and determination. During the collection period, ambient air was drawn to the system at a flow rate of 10 L/min. GOM and PBM in the air were captured by a KCl-coated quartz annular denuder in the 1130 unit and a quartz filter in the 1135 unit, respectively, whereas GEM would pass through the denuder and filter and be quantified on the Tekran 2537B by cold-vapor atomic fluorescence spectroscopy (CVAFS). After an hour of sampling, the 1135 quartz filter and the 1130 denuder would be switched to the thermal decomposition mode at 800 ℃ and 500 ℃, respectively, with the resulting Hg^0 quantified by the 2537B unit in the next hour, while the 1135 and 1130 components were flushed with zero-mercury gas for the next sampling.

The instrument maintenance followed typical protocols used in similar studies (Landis et al., 2002;Hu et al., 2014). The quartz annular denuder was recoated every two weeks, the quartz filter was replaced once a month, and the Teflon filter (pore size 0.2 μm) in the sample inlet was changed every two weeks. Automated recalibration of the Tekran 2537B was performed every 25 h using an internal mercury permeation source. No calibration standards were available for GOM and PBM, but the 1σ

143 precision for GOM and PBM was about 15 % (Landis et al., 2002). The detection

144 limit in ambient air is about 0.5 ng m^{-3} for GEM (or TGM) at a resolution of 5 min,

145 and 1 pg m^{-3} for GOM and PBM at a resolution of 2 h (Gustin et al., 2015). Although

146 the Tekran-based mercury speciation technique has been widely used around the

147 world, recent studies have shown that the technique does not efficiently collect all

148 gaseous oxidized mercury and thus may substantially underestimate the concentration

149 of reactive mercury (Huang et al., 2013;Gustin et al., 2013). Therefore, the GOM

150 values reported in this study should be considered as the lower limit of gaseous

151 oxidized mercury in the air (Wang et al., 2014).

152

153 **2.3 Ancillary Data**

154 Standard meteorological measurements including air temperature, air pressure,

155 RH, wind direction and speed were observed with a 5-min resolution. CO was

156 measured by an automated infrared carbon monoxide analyzer (Model EC9830T,

157 Ecotech Inc., Australia), with a detction limit of 40 ppbv. O$_3$ was measured every 5

158 min by an ozone analyzer (Model EC9810B, Ecotech Inc., Australia); its detection

159 limit and accuracy are 0.5 ppbv and 0.001 ppm, respectively. NO$_2$ was measured by a

160 Multi axis differential optical absorption spectroscopy (MAX-DOAS) instrument. The

161 collected spectra were analyzed using the QDOAS spectral fitting software suite

162 developed at BIRA-IASB (http://uv-vis.aeronomie.be/software/QDOAS/). PM$_{2.5}$

163 (particulate matter less than 2.5 μm in diameter) data are collected from China air

164 quality online analysis platform (http://www.aqistudy.cn/historydata/index.php).

165

166 **2.4 Potential Sources Contribution Function (PSCF) analysis**

167   To identify the possible influence of long-range transport on the distribution of

168   atmospheric mercury in Hefei, we calculated backward trajectories of air masses

169   using the HYSPLIT (Hybrid Single-particle Lagrangian Integrated Trajectory) model

170   with the Global Data Assimilation System (GDAS 1°) developed by the National

171   Oceanic and Atmospheric Administration (NOAA) (*http://www.ready.noaa.gov*)

172   (Draxler and Hess, 1998). Considering the atmospheric pollutants are mainly

173   concentrated in the low altitude during heavy pollution days, the trajectory arrival

174   heights were set at 500 m to represent the boundary layer where atmospheric

175   pollutants were well mixed. In this study, 3-day back-trajectories were generated

176   hourly by TrajStat, a software including HYSPLIT for trajectory calculation (Wang et

177   al., 2009).

178   The contributions of other pollution source regions to the atmospheric mercury at

179   Hefei was identified by the Potential Sources Contribution Function (PSCF) analysis

180   with the TrajStat software. PSCF analysis has been shown to be useful in spatially

181   identifying pollution sources for pollutants with a long lifetime such as elemental

182   mercury and CO (Xu and Akhtar, 2010). The PSCF values for the grid cells in the

183   study domain were calculated by counting the trajectory segment endpoints that

184   terminate within each cell. The number of endpoints that fall in the ij_{th} cell is

185   designated as N_{ij}. The number of endpoints for the same cell corresponding to the

186   atmospheric mercury concentration higher than an arbitrarily set criterion is defined to

187   be M_{ij}. In this study, mean GEM concentration of 4 ng m^{-3} during the whole study

188   period was used as the mercury pollution criterion. The PSCF value for the ij_{th} cell is

189   then defined as:

190    $$PSCF_{ij} = \frac{M_{ij}}{N_{ij}} W_{ij} \qquad\qquad\qquad (2)$$

191   W_{ij} is an arbitrary weight function to reduce the effect of small values of N_{ij}. The

192   PSCF values were multiplied by W_{ij} to better reflect the uncertainty in the values for

193   these cells (Polissar et al., 2001). The weight function reduces the PSCF values when

194   the total number of endpoints in a particular cell is less than 3 times the average value

195   of the end points per cell:

196
$$W_{ij} = \begin{cases} 1.0 & N_{ij} \geq 3N_{ave} \\ 0.70 & 3N_{ave} > N_{ij} \geq 1.5N_{ave} \\ 0.40 & 1.5N_{ave} > N_{ij} \geq N_{ave} \\ 0.20 & N_{ave} > N_{ij} \end{cases} \qquad (3)$$

197

198   **3.   Results**

199   We intended to continuously monitor speciated atmospheric mercury

200   concentration over the course of a year; however, interruptions were inevitable due to

201   instrument maintenance, which resulted in loss of data for the following four periods:

202   (1) 25 September to 9 October 2013; (2) 5-14 November 2013; (3) 9-25 February

203   2014; and (4) 1-14 April 2014. The rest of the data were grouped into haze days and

204   non-haze days according to the China Meteorological Administration's haze standard

205   (QX/T 113-2010). Haze days refer to the days when the atmospheric visibility < 10

206   km and RH < 80% (Duan et al., 2016), and non-haze days refer to clear days with the

207   atmospheric visibility > 10 km. The visibility and RH information were collected

208   from the weather history data at the Luogang Airport of Hefei

209   (http://www.wunderground.com/). Through the study period of almost a year, a total

210   of 56 days were identified to be haze days, and 253 days to be non-haze days. All the

211   times reported herein are local time (UTC + 8 h).

212

213   **3.1 Overall characteristics of speciated atmospheric mercury**

214   The time series of GEM, GOM and PBM concentrations at the study site

215   throughout the study period are shown in Fig. 2, and their frequency distributions are

216   shown in Fig. S1 (in the supporting information). The mean ($\pm$ standard deviation)

217   GEM, GOM and PBM concentrations during the whole study period were 4.07 ± 1.91

218   ng m^{-3}, 3.67 ± 5.11 pg m^{-3}, and 30.0 ± 100.3 pg m^{-3}, respectively (Table 1). The GEM

219   concentrations in different seasons did not differ much. The highest GEM

220   concentration occurred in autumn (4.51 ± 2.10 ng m^{-3}), while the lowest in spring

221   (3.89 ± 1.79 ng m^{-3}). GOM concentrations varied greatly during the study period with

222   much higher concentrations in autumn and the lowest in winter. A similar seasonal

223   variation in the GOM concentration was observed at a remote site in Mt. Gongga of

224   southwest China (Fu et al., 2008b). The seasonal trend in PBM was also observed in

225   Hefei with its concentration decreasing in the following order: autumn > winter >

226   spring > summer. The mean PBM concentration during the cold season was about 20

227   times that in summer, similar to the findings from many previous studies in China

228   (Zhang et al., 2013;Fu et al., 2011;Fu et al., 2008b;Fang et al., 2001).

229   Comparisons of speciated atmospheric mercury concentrations with other urban

230   and rural areas in China and a few other countries are shown in Table 2. The mean

231   GEM concentration at Hefei is slightly higher than that in many remote areas in China

232   (Fu et al., 2008a;Fu et al., 2008b;Fu et al., 2012;Wan et al., 2009a;Wan et al.,

233   2009b;Zhang et al., 2015a), but is much lower than those in urban areas of industrial

234   cities such as Guiyang and Changchun where large point sources of mercury exist

235   (e.g., non-ferrous metal smelting, coal-fired power plants, and residential coal burning)

236   (Feng et al., 2004;Fu et al., 2011;Fang et al., 2004). Although Hefei is geographically

237   close to Shanghai, a mega urban centre in China, it is interesting to note that the TGM

238　concentration of Shanghai is much lower than that of Hefei. This may be due to the

239　fact that Shanghai is a coastal city that is influenced more by cleaner marine air

240　masses (Friedli et al., 2011). Table 2 also shows that the average concentration of

241　GEM in Hefei is typically more than fold or two-fold that in the urban and rural areas

242　in Europe and North America (Liu et al., 2010;Li et al., 2008;Brooks et al., 2010).

243

244　**3.2 Speciated atmospheric mercury during non-haze days**

245　　The frequency distribution of GEM, GOM and PBM for the non-haze period are

246　shown in Fig. S1 (in blue). The mean concentration of GEM was 3.95 ± 1.93 ng m^{-3}.

247　Its distribution was characterized by large fluctuations ranging from 0.2 to 23.8 ng

248　m^{-3}, although more than half of the GEM values were in the narrow range 2-4 ng m^{-3}.

249　The mean concentration of GOM was 2.49 ± 2.41 pg m^{-3} with a range of 0.5-33.5 pg

250　m^{-3}, although most of the values were in the range of 1-4 pg m^{-3}. High concentrations

251　of GOM (exceeding 10 pg m^{-3}) only accounted for 1.4% of the total data. The mean

252　GOM concentration at the Hefei site is much smaller than that reported from other

253　study sites in China (Table 2), but is comparable to the values observed from many

254　European and North American sites (Peterson et al., 2012;Cheng et al., 2014;Ren et

255　al., 2016). The mean PBM concentraion at the Hefei site during the non-haze days

256　was 23.3 ± 90.8 pg m^{-3} with an exceptionally large range of 0.5-1827 pg m^{-3}. The

257　frequency distribution of PBM showed that high PBM concentrations (i.e., > 50 pg

258　m^{-3}) accounted for 6.4% of the total data. The PBM concentration under the non-haze

259　condition in Hefei is generally at a similar level to the remote areas, such as Mt.

260　Gongga, Mt. Waliguan and Shangri-La in western China.

261   Diurnal variations of GEM, PBM and GOM concentrations for non-haze days are

262   shown in Fig. 3. Both GEM and PBM concentrations exhibited similar variations with

263   elevated concentrations during night. The GOM concentration during the daytime was

264   slightly higher than that in nighttime, typically peaking between 10:00 and 12:00.

265

266   **3.3 Speciated atmospheric mercury during haze days**

267   Haze pollution mainly occurred in December and January at our monitoring site.

268   The four major haze pollution periods were identified in grey in Fig. 2. The mean

269   concentrations of GEM, GOM and PBM during these haze days were 4.74 $\pm$ 1.62 ng

270   m^{-3}, 4.32 $\pm$ 8.36 pg m^{-3} and 60.2 $\pm$ 131.4 pg m^{-3}, respectively (Table 1). The frequency

271   distributions of GEM, GOM and PBM for the haze days are shown in Fig. S1 (in

272   gray). Comparison of GEM, GOM and PBM concentrations during haze and non-haze

273   days is shown in Fig. S2. GEM, GOM and PBM concentrations show siginificant

274   differences between haze and non haze days (p<0.001, t-test). On average, the

275   concentration of GEM in haze days was 1.2 times that in non-haze days. Similarly, the

276   concentration of GOM in haze days was about 1-1.7 times those in non-haze days.

277   The largest impact of haze pollution is however on PBM, with the mean PBM

278   concentration in haze days about 2.5 times that of non-haze days. High concentrations

279   of GOM (exceeding 10 pg m^{-3}) and PBM concentrations (exceeding 50 pg m^{-3}) were

280   also more frequently observed than in non-haze days, accounting for 5.9% and 25%,

281   respectively, of the total haze days.

282   Diurnal variations of GEM, PBM and GOM concentrations for haze days are

283   shown in Fig. 3. GEM concentrations were higher during night, decreased during

284   daytime. The opposite pattern was observed for GOM, which showed higher

285   concentrations during daytime than during night; the duration of the GOM peak also

286   lasted longer for haze days. On the contrary, the PBM typically peaked just before

287   sunrise, with the lowest values occurred in the afternoon (14:00-16:00).

288

289   **4.   Discussion**

290   **4.1 Influence of atmospheric mercury emission source**

291   In order to understand the mercury sources attribution, the PSCF model analysis

292   was conducted by using the TrajStat software. The seasonal sources could be inferred

293   from the PSCF analysis with the year-round data. Fig. 4a showed the overall spatial

294   contribution of mercury emission sources in China. As Hefei is located in east-central

295   China, its atmospheric mercury concentration could be affected by both north and

296   south emission sources, including those from the North China Plain (especially

297   Shandong Provice) and the neighboring provinces of Henan, Jiangsu, Jiangxi and

298   Hubei. The total mercury emissions from Henan and Shandong provinces were

299   estimated to be over 50 and 45 tons in 2010, respectively, making them two largest Hg

300   emitters in China (Zhang et al., 2015b). Long-range transport could also impact the

301   seasonal variations of atmospheric mercury in Hefei. As shown in Figure 4, in spring,

302   the major contributors of atmospheric mercury to Hefei were from the southwestern

303   region including the local area and the Jiangxi and Hunan provinces. In summer, the

304   main contributors were from north of Anhui, as well as Henan and Jiangxi provinces,

305   and even from the Pearl River Delta region in the far south. Since the number of haze

306   days accounts only for 5.6% of the total days in spring and summer, we did not

307   provide haze and non-haze PSCF results for spring and summer seasons. As autumn

308   and winter are the prevalent seasons for haze pollution, one PSCF result for haze days

309 and another for non-haze days are shown for autumn and winter, respectively. The

310 statistically significant difference (p<0.001) in the GEM concentration between

311 non-haze days and haze days suggests that haze pollution could directly affect the

312 concentration of elemental mercury. As shown in Figs. 4d and 4f, higher GEM

313 concentration was mainly influenced by local emission sources during haze days. For

314 non-haze days, the most important mercury sources to the monitoring site were not

315 only the local emission sources, but also those from the neighboring region of

316 Shandong, Henan and Jiangxi provinces (see Figs. 4e and 4g). In summary, the

317 increase of GEM concentration during haze days was mainly caused by local

318 emission.

319   GEM and CO often share anthropogenic emission sources, such as industrial coal

320 combustion, domestic coal combustion, iron and steel production and cement

321 production (Wu et al., 2006;Wang et al., 2005). However, they also have their own

322 sources. For instance, power plants and nonferrous metal smelters emit mercury but

323 hardly any CO, while most of CO originates from vehicles which are not a major

324 emitter for mercury. The correlation coefficients and slopes between GEM

325 concentration and CO concentration during pollution events are shown in Table 3.

326 These mercury pollution episodes were defined as a period with hourly average GEM

327 concentration higher than seasonal average GEM concentration and the duration of

328 elevated hourly GEM concentration lasted for over 10 hours. The Hg/CO slope and

329 correlation between GEM and CO concentrations has been used to identify long-range

330 transport episodes and local episodes in previous research (Jaffe et al.,

331 2005;Weiss-Penzias et al., 2006;Kim et al., 2009). These episodes could classified

332 into long-range transport episodes or local episode by using the correlation

14

coefficients (R^2) of linear regression: significant positive correlation for long-range transport episodes and poor correlation for local episodes (Kim et al., 2009). Six episodes (events: 1-6) were found to have poor correlations between GEM and CO concentrations (R^2: 0.01-0.29) for local episodes, while four episodes (events: 7-10) were found to have positive correlations between GEM and CO concentrations (R^2: 0.51-0.79) for long-range transport episodes. These local episodes tend to occur in autumn and winter. The slope of the trend line represents the Hg/CO ratio. Emissions from power plants typically have a higher Hg/CO ratio (Wu et al., 2006), whereas residential coal and biomass burning combustion have a lower Hg/CO ratio (0.0013-0.0046 ng m^{-3} $ppbv^{-1}$) due to incomplete combustion (Weiss-Penzias et al., 2007). The Hg/CO ratio for vehicles is nearly zero (Zhang et al., 2013). The Hg/CO ratios from our study for pollution episodes are in the range of 0.0001-0.0050 ng m^{-3} $ppbv^{-1}$. In summary, the low GEM/CO ratio in Hefei might related to the local incomplete combustion, like residential coal and biomass burning combustion.

4.2 Impacts of meteorological factors for atmospheric mercury during haze days

Meteorological conditions, especially wind direction and speed, could also impact the atmospheric mercury during haze days. The wind rose for the monitoring site during the study period is shown in Fig. 5. Easterly and southeasterly winds represented the prevailing wind directions at the study site. A wind rose diagram of GEM concentrations above the 90th percentile value is shown in Fig. 5B. We found that 67% of the high GEM concentrations occurred at low wind speed (below 1.5 m s^{-1}); however, wind speed below 1.5 m s^{-1} accounted for only 1.7% of total study. High GOM and PBM concentrations appear not to be related to high wind speed

357 (wind speed: 3-5 m s^{-1}); only 1.4% and 2.6% of the high GOM and PBM

358 concentrations were observed under high wind-speed conditions, respectively (Figs.

359 5C and 5D). In general, most of the high atmospheric mercury levels occurred in the

360 low wind speed conditions. This slow wind speed condition is not conductive to the

361 spread of mercury and thus favours the accumulation of atmospheric mercury,

362 especially during haze days. This result is further support that atmospheric mercury

363 during haze days is mainly affected by local emissions.

364   Both GEM and PBM concentrations exhibited great variations with elevated

365 concentration during night or early morning, regardless of the presence of haze. Such a

366 diurnal variation of GEM and PBM could be related to changes in the height of urban

367 boundary layer, which is typically low in the morning and night, and high during the

368 daytime (Yuan et al., 2005;Mao et al., 2006). The maximum PBM concentration

369 (observed at 6:00) was more than 4 times higher than the minimum value (observed at

370 16:00) both under non-haze and haze days, and about 76% PBM were declined during

371 this period (6:00-16:00). However, the reductions of PBM as a result of deposition

372 during haze days was 62.7 pg m^{-3}, which was about 2.4 times that in non-haze days,

373 suggesting that haze pollution could increase the removal of PBM and thus reduce its

374 atmospheric lifetime. Although PBM is not the major form of mercury emitted to the

375 atmosphere, it is crucial in atmospheric mercury transport and removal processes due to

376 its short atmospheric lifetime. As shown in Fig. 6, highest PBM and PM$_{2.5}$

377 concentrations were observed in January, which most likely due to shallower boundary

378 layer in January than in other months. The co-variation in February is weaker, possibly

379 due to the loss of PBM data because of instrument maintenance (see Section 2.3). The

380 PBM concentration co-varied with the PM$_{2.5}$ concentration, especially in January when

381 all the four PBM peak events were associated with increased PM$_{2.5}$ concentrations (Fig.

382 6c). This result indicates that the PM$_{2.5}$ concentration may play an important role in the

383 formation of PBM. Thus, elevated PBM concentrations might be due to the poor

384 diffusion conditions in cold months and high PM pollution.

385

386 **4.3 Enhancements in GOM and the potential oxidation mechanism**

387 Diurnal variations of GEM, GOM, O$_3$ and CO concentrations during non-haze

388 and haze days are shown in Fig. 7. The weak correlation (r=0.164, p<0.001) between

389 GOM and CO suggests that the CO-producing, primary emission is not a major source

390 of GOM in the air. This is clearly shown in Fig. 7 (haze days), where the peak value

391 of GOM coincided with the lowest value of CO. GOM also shows a diurnal trend that

392 is opposite to that of GEM and PBM; for both non-haze and haze days, GOM

393 concentrations remained relatively constant during night, but increased rapidly prior

394 to sunrise. Two processes can affect the GOM concentrations in the boundary layer air.

395 The first is due to transport of GOM from the free troposphere (FT). It is well

396 established that FT contains higher GOM concentrations than in the boundary

397 layer(e.g., (Murphy et al., 2006;Lyman and Jaffe, 2012;Timonen et al., 2013;Brooks

398 et al., 2014;Shah et al., 2016)). It is thus possible that higher GOM concentrations

399 observed prior to sunrise is due to admixing from the free troposphere as the height of

400 the boundary layer increases during the morning. In addition, in situ photochemical

401 oxidation of GEM could also increase the concentration of GOM during daytime.

402 Various atmospheric oxidants are capable of oxidizing GEM to GOM, including

403 halogen radicals, ozone, hydroxyl radicals (OH), among others (Holmes et al.,

404 2010;Wang et al., 2014).

To determine the relative importance of FT transport and in situ photochemical oxidation, we examined the relationship between GOM and the changes in the height of the atmospheric boundary layer and the odd oxygen ($O_X = O_3 + NO_2$) concentrations. We used O_x because it is a more conserved tracer of the extent of photochemical processes in the urban atmosphere (Herndon et al., 2008;Wood et al., 2010), as O_3 reacts with NO emitted from automobiles to form NO_2. Example results are shown in Fig. 8 for 20th November, 2013. As can be seen from the figure, both GOM and O_X reached higher concentrations from 12:00 to 16:00, along with the lowest value of GEM. The height of the atmospheric boundary layer changed very little (less than 0.1 km) over the same period (see Fig. S3). This simple comparison suggests that the transport of FT GOM might be limited and that at least some of the GOM were formed from in situ oxidation of GEM. Note that in our studies we could only calculate daytime O_x concentrations, because NO_2 concentrations from MAX-DOAS were only available during daytime.

We further investiagted the mechanism of the GEM oxidation to GOM. Ozone itself is not an efficient oxidant for GEM oxidation due to the low reaction rate (Hall, 1995;Holmes et al., 2010). Instead, halogen radicals (especially bromine atoms) and halogen radicals, are believed to be the primary oxidants for GEM in the global troposphere (Holmes et al., 2010). Unfortunately, we did not measure halogen radicals in this study. OH radicals are known to be present in the early morning urban boundary layer, primarily from the photolysis of HONO, which accumulates during night (Kleffmann et al., 2005). Therefore, here we consider the oxdiation of GEM by OH radicals. The formation of HgOH as an intermediate product of the $Hg^0(g) + OH$ oxidation reactions has been proposed by Sommar et al., 2001, although HgOH is

429   highly unstable and could decompose back rapidly to Hg^0 and OH (Sommar et al.,

430   2001;Goodsite et al., 2004). It has been proposed that the presence of other gases X

431   (X = NO_2, HO_2, RO, RO_2, or NO) could assist the formation of Hg(II) by forming

432   X-HgOH, which outcompetes the decomposition of HgOH (Calvert and Lindberg,

433   2005;Dibble et al., 2012;Wang et al., 2014). As an example, we calculated the

434   transformation between GEM and GOM under the influence of NO_2, using the

435   reactions and rate constants shown in Table S1. As shown in Fig. S4, the production

436   rate of NO_2HgOH, d[NO_2HgOH]/dt, increased almost linearly with increasing NO_2

437   under low NO_2 concentrations, and eventually reached a steady state when the NO_2

438   concentration is high enough.

439   Based on the production rate of NO_2HgOH, we can estimate the production of

440   NO_2HgOH during the 1 hr sampling period when GOM was captured by the

441   KCl-coated denuder in the Tekran 1130 unit. The production of NO_2HgOH and

442   d[NO_2HgOH]/dt corresponding to different NO_2 concentrations is shown in Table 4.

443   With the increase of the NO_2 concentration, the contribution of the NO_2HgOH

444   production to GOM will increase. If the NO_2 concentration is within 100 ppbv (from

445   0 to 100 ppbv), the production of NO_2HgOH would be in range of 0.058-4.81 pg m^{-3}

446   during the 1h sampling period. As illustrated in Table 4, the level of NO_2 observed in

447   our study is high enough to make increase the GOM production. Our results thus

448   support a recent study in the tropical equatorial Pacific (Wang et al., 2014) that NO_2

449   aggregation with HgOH provides provides a possible mechanism to explain the

450   enhanced production of GOM and the role of NO_2 might be more important in the

451   urban air. More laboratory and modeling studies on mercury oxidation mechanism in

452   the presence of NO_2 and other gases are thus warranted.

5. Summary

Continuous measurements of speciated atmospheric mercury were conducted at Hefei, a mid-latitude inland city in central China, from July 2013 to June 2014. Measurements of other trace gases (e.g. CO, O_3, NO_2) and meteorological parameters were employed to better understand the sources and oxidation pathways of atmospheric mercury. The mean GEM, GOM and PBM concentrations during haze days were 4.74 ± 1.62 ng m^{-3}, 4.32 ± 8.36 pg m^{-3} and 60.2 ± 131.4 pg m^{-3}, respectively. Potential source contribution function (PSCF) analysis suggested that the local mercury emission rather than long-range transport is the most important contributor of atmospheric mercury pollution during haze days at our monitoring site. The low GEM/CO ratio in Hefei could be a result of local incomplete combustion sources such as residential coal and biomass burning. Haze pollution has a more profound impact on PBM than on GEM and GOM. PBM showed a remarkable seasonal pattern, with higher concentrations in cold seasons and lower in warm seasons. Elevated PBM concentrations might be due to both the high loadings of particle matter and disadvantageous diffusion conditions during haze days especially in cold months. Both GEM and PBM concentrations exhibited great variations with elevated concentration during night. The diurnal variations of GEM and PBM might be related to the boundary layer depth; a lower boundary layer depth in the morning and night could elevate the mercury concentration.

Unlike with the diurnal variations of GEM and PBM, GOM concentration remained relatively constant during night, and then increased rapidly prior to the sunrise. The enhancement of GOM during daytime could be due to both the transport of GOM-enriched free troposphere air to the boundary layer and in situ oxidation of

GEM in the boundary layer. Simple photochemical modeling supports the occurrence of daytime oxidation of GEM to GOM. Based on HgOH as an intermediate product, our calculations suggest that NO_2 aggregation with HgOH is a potential mechanism to explain the enhanced production of GOM over the inland urban air.

489 **References**

490 Brooks, S., Luke, W., Cohen, M., Kelly, P., Lefer, B., and Rappenglück, B.: Mercury

491   species measured atop the Moody Tower TRAMP site, Houston, Texas,

492   Atmospheric Environment, 44, 4045-4055, 2010.

493 Brooks, S., Ren, X., Cohen, M., Luke, W. T., Kelley, P., Artz, R., Hynes, A., Landing,

494   W., and Martos, B.: Airborne vertical profiling of mercury speciation near

495   Tullahoma, TN, USA, Atmosphere, 5, 557-574, 2014.

496 Calvert, J. G., and Lindberg, S. E.: Mechanisms of mercury removal by O_3 and OH in

497   the atmosphere, Atmospheric Environment, 39, 3355-3367, 2005.

498 Chen, L.-W. A., Chow, J. C., Doddridge, B. G., Dickerson, R. R., Ryan, W. F., and

499   Mueller, P. K.: Analysis of a summertime $PM_{2.5}$ and haze episode in the

500   mid-Atlantic region, Journal of the Air & Waste Management Association, 53,

501   946-956, 2003.

502 Cheng, I., Zhang, L., Mao, H., Blanchard, P., Tordon, R., and Dalziel, J.: Seasonal and

503   diurnal patterns of speciated atmospheric mercury at a coastal-rural and a

504   coastal-urban site, Atmospheric Environment, 82, 193-205, 2014.

505 Dibble, T., Zelie, M., and Mao, H.: Thermodynamics of reactions of ClHg and BrHg

506   radicals with atmospherically abundant free radicals, Atmospheric Chemistry and

507   Physics, 12, 10271-10279, 2012.

508 Draxler, R. R., and Hess, G.: An overview of the HYSPLIT_4 modelling system for

509   trajectories, Australian meteorological magazine, 47, 295-308, 1998.

510 Duan, L., Xiu, G., Feng, L., Cheng, N., and Wang, C.: The mercury species and their

511   association with carbonaceous compositions, bromine and iodine in $PM_{2.5}$ in

512   Shanghai, Chemosphere, 146, 263-271, 2016.

513   Fang, F., Wang, Q., and Li, J.: Atmospheric particulate mercury concentration and its

514   dry deposition flux in Changchun City, China, Science of the total environment, 281,

515   229-236, 2001.

516   Fang, F., Wang, Q., and Li, J.: Urban environmental mercury in Changchun, a

517   metropolitan city in Northeastern China: source, cycle, and fate, Science of the Total

518   Environment, 330, 159-170, 2004.

519   Fang, G.-C., Wu, Y.-S., and Chang, T.-H.: Comparison of atmospheric mercury (Hg)

520   among Korea, Japan, China and Taiwan during 2000-2008, Journal of hazardous

521   materials, 162, 607-615, 2009.

522   Feng, X., Shang, L., Wang, S., Tang, S., and Zheng, W.: Temporal variation of total

523   gaseous mercury in the air of Guiyang, China, Journal of Geophysical Research:

524   Atmospheres (1984-2012), 109, 2004.

525   Friedli, H., Arellano Jr, A., Geng, F., Cai, C., and Pan, L.: Measurements of

526   atmospheric mercury in Shanghai during September 2009, Atmospheric Chemistry

527   and Physics, 11, 3781-3788, 2011.

528   Fu, X., Feng, X., Zhu, W., Wang, S., and Lu, J.: Total gaseous mercury concentrations

529   in ambient air in the eastern slope of Mt. Gongga, South-Eastern fringe of the

530   Tibetan plateau, China, Atmospheric Environment, 42, 970-979, 2008a.

531   Fu, X., Feng, X., Zhu, W., Zheng, W., Wang, S., and Lu, J. Y.: Total particulate and

532   reactive gaseous mercury in ambient air on the eastern slope of the Mt. Gongga area,

533   China, Applied Geochemistry, 23, 408-418, 2008b.

534   Fu, X., Feng, X., Qiu, G., Shang, L., and Zhang, H.: Speciated atmospheric mercury

535   and its potential source in Guiyang, China, Atmospheric Environment, 45,

536   4205-4212, 2011.

537   Fu, X., Feng, X., Liang, P., Zhang, H., Ji, J., and Liu, P.: Temporal trend and sources of

538   speciated atmospheric mercury at Waliguan GAW station, Northwestern China,

539   Atmospheric Chemistry and Physics, 12, 1951-1964, 2012.

540   Goodsite, M. E., Plane, J., and Skov, H.: A theoretical study of the oxidation of Hg^0 to

541          $HgBr_2$ in the troposphere, Environmental science & technology, 38, 1772-1776,

542   2004.

543   Gustin, M., and Jaffe, D.: Reducing the uncertainty in measurement and understanding

544   of mercury in the atmosphere, Environmental science & technology, 44, 2222-2227,

545   2010.

546   Gustin, M., Amos, H., Huang, J., Miller, M., and Heidecorn, K.: Measuring and

547   modeling mercury in the atmosphere: a critical review, Atmospheric Chemistry and

548   Physics, 15, 5697-5713, 2015.

549   Gustin, M. S., Huang, J., Miller, M. B., Peterson, C., Jaffe, D. A., Ambrose, J., Finley, B.

550   D., Lyman, S. N., Call, K., and Talbot, R.: Do we understand what the mercury

551   speciation instruments are actually measuring? Results of RAMIX, Environmental

552   science & technology, 47, 7295-7306, 2013.

553   Hall, B.: The gas phase oxidation of elemental mercury by ozone, in: Mercury as a

554   Global Pollutant, Springer, 301-315, 1995.

555   Herndon, S. C., Onasch, T. B., Wood, E. C., Kroll, J. H., Canagaratna, M. R., Jayne, J.

556   T., Zavala, M. A., Knighton, W. B., Mazzoleni, C., and Dubey, M. K.: Correlation of

557   secondary organic aerosol with odd oxygen in Mexico City, Geophysical Research

558   Letters, 35, 2008.

559 Holmes, C. D., Jacob, D. J., Corbitt, E. S., Mao, J., Yang, X., Talbot, R., and Slemr, F.:

560 Global atmospheric model for mercury including oxidation by bromine atoms,

561 Atmospheric Chemistry and Physics, 10, 12037-12057, 2010.

562 Hu, Q. H., Kang, H., Li, Z., Wang, Y. S., Ye, P. P., Zhang, L. L., Yu, J., Yu, X. W., Sun,

563 C., and Xie, Z. Q.: Characterization of atmospheric mercury at a suburban site of

564 central China from wintertime to springtime, Atmospheric Pollution Research, 5,

565 769-778, 2014.

566 Huang, J., Miller, M. B., Weiss-Penzias, P., and Gustin, M. S.: Comparison of gaseous

567 oxidized Hg measured by KCl-coated denuders, and nylon and cation exchange

568 membranes, Environmental science & technology, 47, 7307-7316, 2013.

569 Jaffe, D., Prestbo, E., Swartzendruber, P., Weiss-Penzias, P., Kato, S., Takami, A.,

570 Hatakeyama, S., and Kajii, Y.: Export of atmospheric mercury from Asia,

571 Atmospheric Environment, 39, 3029-3038, 2005.

572 Kim, S.-H., Han, Y.-J., Holsen, T. M., and Yi, S.-M.: Characteristics of atmospheric

573 speciated mercury concentrations (TGM, Hg (II) and Hg (p)) in Seoul, Korea,

574 Atmospheric Environment, 43, 3267-3274, 2009.

575 Kleffmann, J., Gavriloaiei, T., Hofzumahaus, A., Holland, F., Koppmann, R., Rupp, L.,

576 Schlosser, E., Siese, M., and Wahner, A.: Daytime formation of nitrous acid: A

577 major source of OH radicals in a forest, Geophysical Research Letters, 32, 2005.

578 Landis, M. S., Stevens, R. K., Schaedlich, F., and Prestbo, E. M.: Development and

579 characterization of an annular denuder methodology for the measurement of

580 divalent inorganic reactive gaseous mercury in ambient air, Environmental science

581 & technology, 36, 3000-3009, 2002.

582   Li, J., Sommar, J., Wängberg, I., Lindqvist, O., and Wei, S.-q.: Short-time variation of

583   mercury speciation in the urban of Göteborg during GÖTE-2005, Atmospheric

584   Environment, 42, 8382-8388, 2008.

585   Lindberg, S., Bullock, R., Ebinghaus, R., Engstrom, D., Feng, X., Fitzgerald, W.,

586   Pirrone, N., Prestbo, E., and Seigneur, C.: A synthesis of progress and uncertainties

587   in attributing the sources of mercury in deposition, AMBIO: A Journal of the

588   Human Environment, 36, 19-33, 2007.

589   Lindqvist, O., and Rodhe, H.: Atmospheric mercury-a review*, Tellus B, 37, 1985.

590   Liu, B., Keeler, G. J., Dvonch, J. T., Barres, J. A., Lynam, M. M., Marsik, F. J., and

591   Morgan, J. T.: Urban-rural differences in atmospheric mercury speciation,

592   Atmospheric Environment, 44, 2013-2023, 2010.

593   Lyman, S. N., and Jaffe, D. A.: Formation and fate of oxidized mercury in the upper

594   troposphere and lower stratosphere, Nature Geoscience, 5, 114-117, 2012.

595   Mao, M., Jiang, W., Wu, X., Qi, F., Yuan, R., Fang, H., Liu, D., and Zhou, J.: LIDAR

596   exploring of the UBL in downtown of the Nanjing City, Acta Scientiae

597   Circumstantiae, 26, 1723-1728, 2006.

598   Marumoto, K., Hayashi, M., and Takami, A.: Atmospheric mercury concentrations at

599   two sites in the Kyushu Islands, Japan, and evidence of long-range transport from

600   East Asia, Atmospheric Environment, 117, 147-155, 2015.

601   Murphy, D., Hudson, P., Thomson, D., Sheridan, P., and Wilson, J.: Observations of

602   mercury-containing aerosols, Environmental science & technology, 40, 3163-3167,

603   2006.

604   Pacyna, E. G., Pacyna, J. M., Steenhuisen, F., and Wilson, S.: Global anthropogenic

605   mercury emission inventory for 2000, Atmospheric environment, 40, 4048-4063,

606   2006.

607   Pacyna, E. G., Pacyna, J., Sundseth, K., Munthe, J., Kindbom, K., Wilson, S.,

608   Steenhuisen, F., and Maxson, P.: Global emission of mercury to the atmosphere

609   from anthropogenic sources in 2005 and projections to 2020, Atmospheric

610   Environment, 44, 2487-2499, 2010.

611   Peterson, C., Alishahi, M., and Gustin, M. S.: Testing the use of passive sampling

612   systems for understanding air mercury concentrations and dry deposition across

613   Florida, USA, Science of the Total Environment, 424, 297-307, 2012.

614   Polissar, A. V., Hopke, P. K., and Harris, J. M.: Source regions for atmospheric aerosol

615   measured at Barrow, Alaska, Environmental science & technology, 35, 4214-4226,

616   2001.

617   Ren, X., Luke, W. T., Kelley, P., Cohen, M. D., Artz, R., Olson, M. L., Schmeltz, D.,

618   Goldberg, D. L., Ring, A., and Mazzuca, G. M.: Atmospheric mercury

619   measurements at a suburban site in the Mid-Atlantic United States: Inter-annual,

620   seasonal and diurnal variations and source-receptor relationships, Atmospheric

621   Environment, 2016.

622   Schroeder, W. H., and Munthe, J.: Atmospheric mercury-an overview, Atmospheric

623   Environment, 32, 809-822, 1998.

624   Shah, V., Jaeglé, L., Gratz, L., Ambrose, J., Jaffe, D., Selin, N., Song, S., Campos, T.,

625   Flocke, F., and Reeves, M.: Origin of oxidized mercury in the summertime free

626   troposphere over the southeastern US, Atmospheric Chemistry and Physics, 16,

627   1511-1530, 2016.

628   Sommar, J., Gårdfeldt, K., Strömberg, D., and Feng, X.: A kinetic study of the

629   gas-phase reaction between the hydroxyl radical and atomic mercury, Atmospheric

630   Environment, 35, 3049-3054, 2001.

631   Streets, D. G., Hao, J., Wu, Y., Jiang, J., Chan, M., Tian, H., and Feng, X.:

632   Anthropogenic mercury emissions in China, Atmospheric Environment, 39,

633   7789-7806, 2005.

634   Sun, Z., Mu, Y., Liu, Y., and Shao, L.: A comparison study on airborne particles during

635   haze days and non-haze days in Beijing, Science of the total environment, 456, 1-8,

636   2013.

637   Timonen, H., Ambrose, J., and Jaffe, D.: Oxidation of elemental Hg in anthropogenic

638   and marine airmasses, Atmospheric Chemistry and Physics, 13, 2827-2836, 2013.

639   Wan, Q., Feng, X., Lu, J., Zheng, W., Song, X., Han, S., and Xu, H.: Atmospheric

640   mercury in Changbai Mountain area, northeastern China I. The seasonal distribution

641   pattern of total gaseous mercury and its potential sources, Environmental research,

642   109, 201-206, 2009a.

643   Wan, Q., Feng, X., Lu, J., Zheng, W., Song, X., Li, P., Han, S., and Xu, H.: Atmospheric

644   mercury in Changbai Mountain area, northeastern China II. The distribution of

645   reactive gaseous mercury and particulate mercury and mercury deposition fluxes,

646   Environmental research, 109, 721-727, 2009b.

647   Wang, F., Saiz-Lopez, A., Mahajan, A., Martń, J. G., Armstrong, D., Lemes, M., Hay,

648   T., and Prados-Roman, C.: Enhanced production of oxidised mercury over the

649   tropical Pacific Ocean: a key missing oxidation pathway, Atmospheric Chemistry

650   and Physics, 14, 1323, 2014.

651   Wang, L., Zhang, Q., Hao, J., and He, K.: Anthropogenic CO emission inventory of

652   Mainland China, Acta Scientiae Circumstantiae, 25, 1580-1585, 2005.

653   Wang, Y., Zhang, X., and Draxler, R. R.: TrajStat: GIS-based software that uses various

654   trajectory statistical analysis methods to identify potential sources from long-term

655   air pollution measurement data, Environmental Modelling & Software, 24, 938-939,

656   2009.

657   Weigelt, A., Temme, C., Bieber, E., Schwerin, A., Schuetze, M., Ebinghaus, R., and

658   Kock, H. H.: Measurements of atmospheric mercury species at a German rural

659   background site from 2009 to 2011-methods and results, Environmental Chemistry,

660   10, 102-110, 2013.

661   Weiss-Penzias, P., Jaffe, D. A., Swartzendruber, P., Dennison, J. B., Chand, D., Hafner,

662   W., and Prestbo, E.: Observations of Asian air pollution in the free troposphere at

663   Mount Bachelor Observatory during the spring of 2004, Journal of Geophysical

664   Research: Atmospheres, 111, 2006.

665   Weiss-Penzias, P., Jaffe, D., Swartzendruber, P., Hafner, W., Chand, D., and Prestbo, E.:

666   Quantifying Asian and biomass burning sources of mercury using the Hg/CO ratio

667   in pollution plumes observed at the Mount Bachelor Observatory, Atmospheric

668   Environment, 41, 4366-4379, 2007.

669   Wood, E., Canagaratna, M., Herndon, S., Onasch, T., Kolb, C., Worsnop, D., Kroll, J.,

670   Knighton, W., Seila, R., and Zavala, M.: Investigation of the correlation between

671   odd oxygen and secondary organic aerosol in Mexico City and Houston,

672   Atmospheric Chemistry and Physics, 10, 8947-8968, 2010.

673 Wu, Y., Wang, S., Streets, D. G., Hao, J., Chan, M., and Jiang, J.: Trends in

674   anthropogenic mercury emissions in China from 1995 to 2003, Environmental

675   science & technology, 40, 5312-5318, 2006.

676 Xu, X., and Akhtar, U.: Identification of potential regional sources of atmospheric total

677   gaseous mercury in Windsor, Ontario, Canada using hybrid receptor modeling,

678   Atmospheric Chemistry and Physics, 10, 7073-7083, 2010.

679 Yuan, S., Xin, Y., and Zhou, J.: Lidar Observations of the Lower Atmosphere in Hefei,

680   Chinese Journal of Atmospheric Sciences, 29, 387-395, 2005.

681 Zhang, H., Fu, X., Lin, C., Wang, X., and Feng, X.: Observation and analysis of

682   speciated atmospheric mercury in Shangri-La, Tibetan Plateau, China, Atmospheric

683   Chemistry and Physics, 15, 653-665, 2015a.

684 Zhang, L., Wang, S., Wang, L., and Hao, J.: Atmospheric mercury concentration and

685   chemical speciation at a rural site in Beijing, China: implications of mercury

686   emission sources, Atmospheric Chemistry and Physics, 13, 10505-10516, 2013.

687 Zhang, L., Wang, S., Wang, L., Wu, Y., Duan, L., Wu, Q., Wang, F., Yang, M., Yang, H.,

688   and Hao, J.: Updated Emission Inventories for Speciated Atmospheric Mercury

689   from Anthropogenic Sources in China, Environmental science & technology, 49,

690   3185-3194, 2015b.

691

692

693 **Table 1. Summary of GEM, GOM and PBM concentrations measured in Hefei**

694 **from July 2013 to June 2014.**

695

	GEM (ng m^{-3})			GOM (pg m^{-3})			PBM (pg m^{-3})		
	Mean$\pm\sigma$	Range	N	Mean$\pm\sigma$	Range	N	Mean$\pm\sigma$	Range	N
Spring	3.89$\pm$1.79	0.2-21.3	7890	4.49$\pm$4.22	0.5-69.8	526	8.34$\pm$8.97	1.6-130.1	542
Summer	4.08$\pm$1.99	0.3-22.9	6050	3.66$\pm$4.39	0.5-45.2	511	3.61$\pm$4.38	0.5-41.9	570
Autumn	4.51$\pm$2.10	0.4-23.8	3632	5.65$\pm$8.93	0.5-78.9	274	59.9$\pm$153.5	0.5-1615	339
Winter	4.05$\pm$1.81	0.9-12.2	6381	2.59$\pm$2.58	0.5-9.5	541	56.1$\pm$134.9	0.5-1827	639
Total	4.07$\pm$1.91	0.2-23.8	23953	3.67$\pm$5.11	0.5-78.9	1852	30.02$\pm$100.3	0.5-1827	2090
Non-haze	3.95$\pm$1.93	0.2-23.8	20345	2.49$\pm$2.41	0.5-33.5	1508	23.3$\pm$90.76	0.5-1827	1708
Haze	4.74$\pm$1.62	2.1-16.5	3608	4.32$\pm$8.36	0.5-78.9	344	60.2$\pm$131.4	1.6-1615	382

696

697

31

Table 2. Speciated atmospheric mercury concentrations in Hefei and other urban and rural areas.

Location	Classification	Time	TGM (ng m^{-3})	GEM (ng m^{-3})	GOM (pg m^{-3})	PBM (pg m^{-3})	Reference
Hefei	Suburb	Jul 2013-Jun 2014	4.1	4.07	3.67	30	This study
Hefei	Suburb	Feb-May 2009	2.53	-	-	-	Hu et al. (2014)
Beijing	Rural	Dec 2008-Nov 2009	3.23	3.22	10.1	98.2	Zhang et al. (2013)
Shanghai	Urban	Aug-Sep 2009	2.7	-	-	-	Friedli et al. (2011)
Nanjing	Urban	Jan-Dec 2011	7.9	-	-	-	Zhu et al. (2012)
Guiyang	Urban	Nov 2001-Nov 2002	8.4	-	-	-	Feng et al. (2004)
Guiyang	Urban	Aug-Dec 2009	-	9.72	35.7	368	Fu et al. (2011)
Changchun	Urban	Jul 1999-Jan 2000	18.4	-	-	276	Fang et al. (2004)
Changchun	Suburb	Jul 1999-Jan 2000	11.7	-	-	109	Fang et al. (2004)
Mt.Changbai	Remote	Aug 2005-Jul 2006	3.58	-	65	77	Wan et al. (2009a, b)
Mt.Gongga	Remote	May 2005-July 2006	3.98	-	6.2	30.7	Fu et al. (2008a, b)
Mt.Waliguan	Remote	Sep 2007-Aug 2008	1.98	-	7.4	19.4	Fu et al. (2012a)
Mt.Leigong	Remote	May 2008-May 2009	2.8	-	-	-	Fu et al. (2010)
Shangri-La	Remote	Nov 2009-Nov 2010	2.55	-	8.22	38.82	Zhang (2015)
Detroit, USA	Urban	Jan-Dec 2004	-	2.5	15.5	18.1	Liu et al. (2010)
Dexter, USA	Rural	Jan-Dec 2004	-	1.6	3.8	6.1	Liu et al. (2010)
Houston, USA	Urban	Aug-Oct 2006	-	1.66	6.9	2.5	Brooks et al. (2010)
Florida, USA	Urban	Jul 2009-Jul 2010		1.3	3	2	Peterson et al. (2012)
Maryland, USA	suburb	2007-2015		1.41	4.6	8.6	Ren et al. (2016)
Göteborg, Sweden	Urban	Feb-Mar 2005	-	1.96	2.53	12.5	Li et al. (2008)
Nova Scotia, Canada	Urban	Jan 2010- Dec 2011		1.67	2.07	2.32	Cheng et al. (2014)
Northern Hemisphere background value				1.5-1.7			Lindberg et al. (2007)

702 **Table 3. Correlation coefficients and slopes between GEM concentration and CO**

703 **concentration during atmospheric mercury pollution events.**

704

Event	Start Time (UTC + 8 hr)	End Time (UTC + 8 hr)	Duration (h)	GEM (ng m^{-3})	CO (ppbv)	GEM/CO (slope, ng m^{-3} ppbv^{-1})	R^2
1	2013/11/21 03:00	2013/11/22 02:00	23	8.37±2.42	4481.6±717.3	0.0018	0.29
2	2013/12/03 20:00	2013/12/04 09:00	13	7.51±0.67	5270.0±744.5	0.0001	0.02
3	2013/12/07 04:00	2013/12/09 04:00	48	9.21±1.16	5943.8±1394.1	0.0004	0.23
4	2013/12/19 09:00	2013/12/20 09:00	24	4.35±0.17	3907.6±353.0	0.0002	0.03
5	2013/12/24 19:00	2013/12/25 15:00	20	5.58±0.94	4930.8±919.7	0.0012	0.01
6	2014/01/17 22:00	2014/01/19 13:00	39	5.80±0.83	5746.3±1626.9	0.0003	0.28
7	2014/01/25 02:00	2014/01/25 22:00	20	6.03±0.50	8797.9±2244.3	0.0002	0.59
8	2014/03/16 05:00	2014/03/16 20:00	15	4.46±0.47	2261.7±440.2	0.0010	0.79
9	2014/03/17 06:00	2014/03/18 12:00	30	8.85±2.46	2697.1±590.3	0.0030	0.51
10	2014/05/21 00:00	2014/05/21 11:00	11	5.74±0.94	3676.7±1690.0	0.0050	0.79

705 Notes: these episodes were identified using the following criteria: (a) the duration of

706 elevated GEM concentration lasted for >10h; (b) the selected hourly average GEM

707 concentration higher than the seasonal average GEM concentration.

708

709

710 **Table 4. The production of NO$_2$HgOH and d[NO$_2$HgOH]/dt at different NO$_2$**

711 **concentrations**

NO2 (ppbv)	10	20	30	40	50	60	70	80	90	100
d(NO$_2$HgOH)/dt (molecule cm^{-3} s^{-1})	0.36	0.71	1.04	1.37	1.68	1.99	2.28	2.56	2.83	3.10
NO2HgOH (pg m^{-3}, 1hr)	0.56	1.10	1.63	2.13	2.61	3.08	3.54	3.97	4.40	4.81

712

713
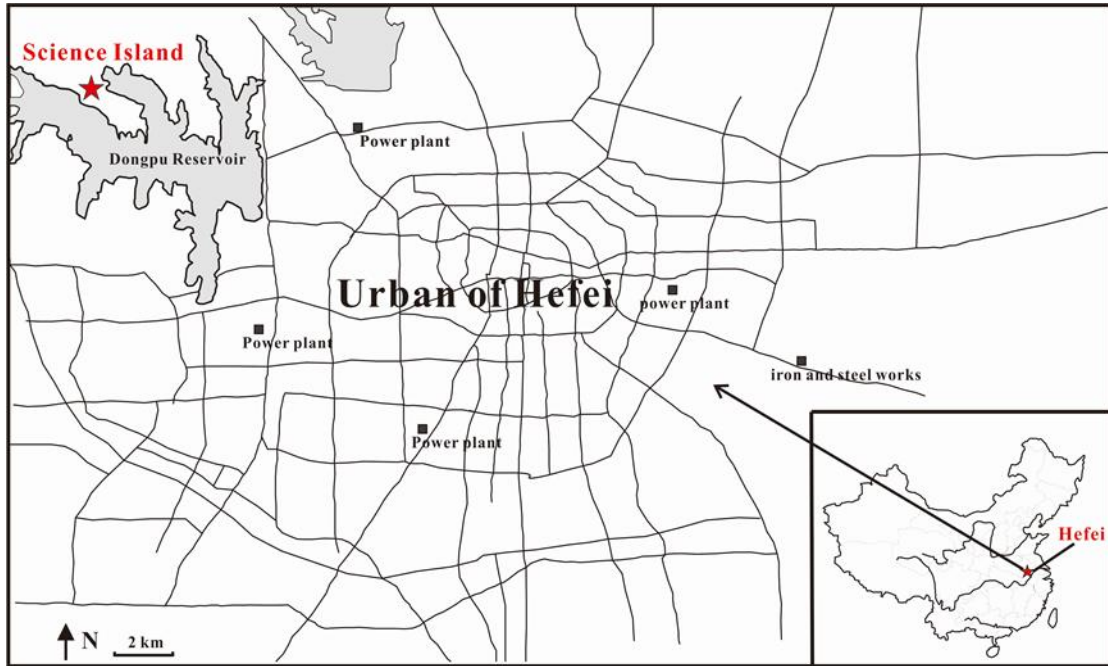
714 **Fig. 1.** Location of the study site in Hefei, China.

715

716
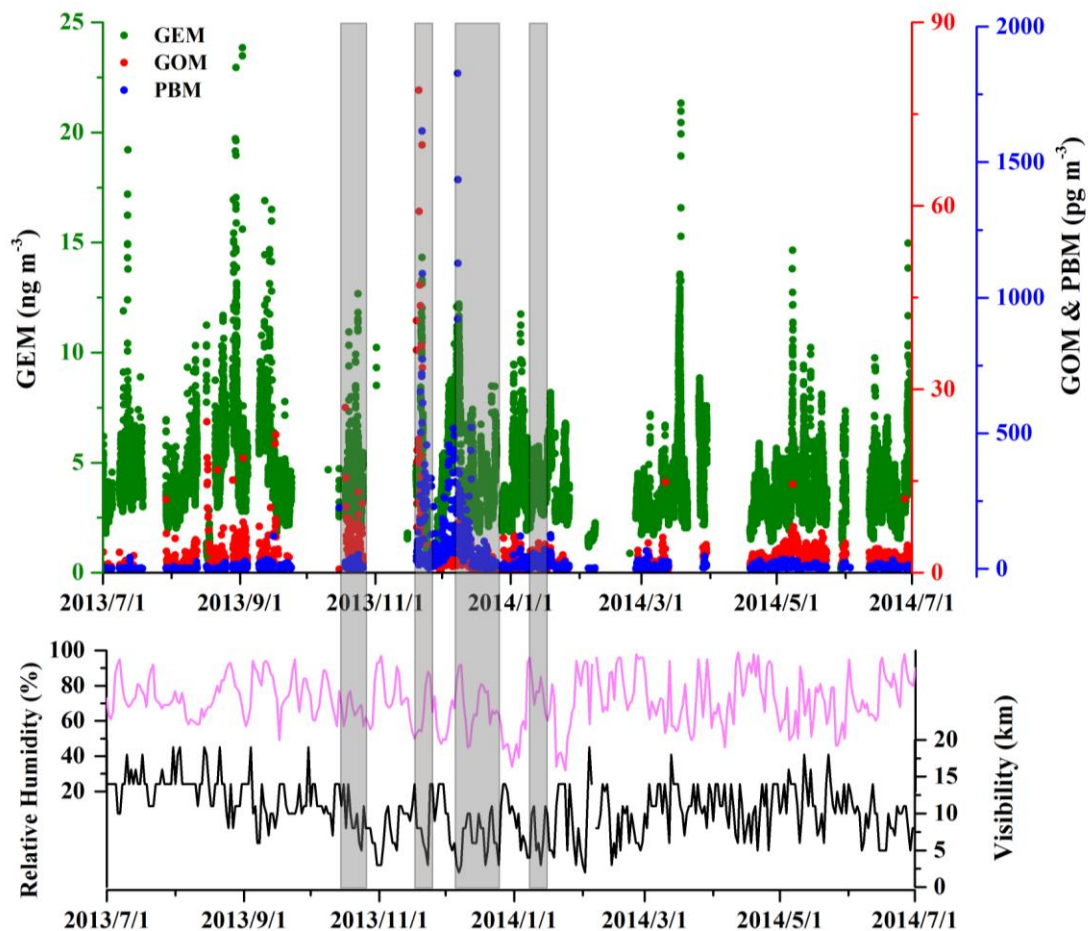
Fig. 2. Time series of GEM, GOM and PBM concentrations, along with visibility,

relatively humidity, at the monitoring site in Hefei from July 2013 to June 2014. The

GEM data were at a 5-min resolution, and the GOM and PBM data were two-hour

averages. The gray columns show the major haze pollution episodes occurred during

the study period.

722
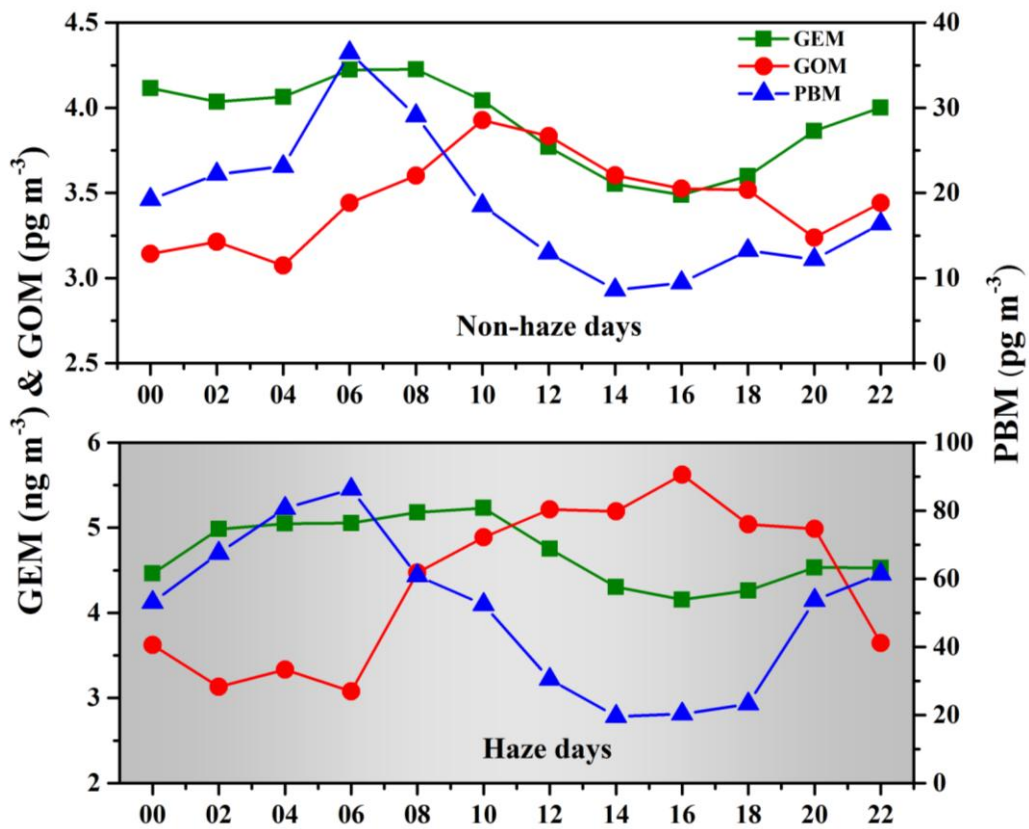
723

724 **Fig. 3.** Diurnal trends of GEM, GOM and PBM concentrations in Hefei during

725 non-haze and haze days (Local time = UTC + 8 hr). The data were two-hour averages.

726
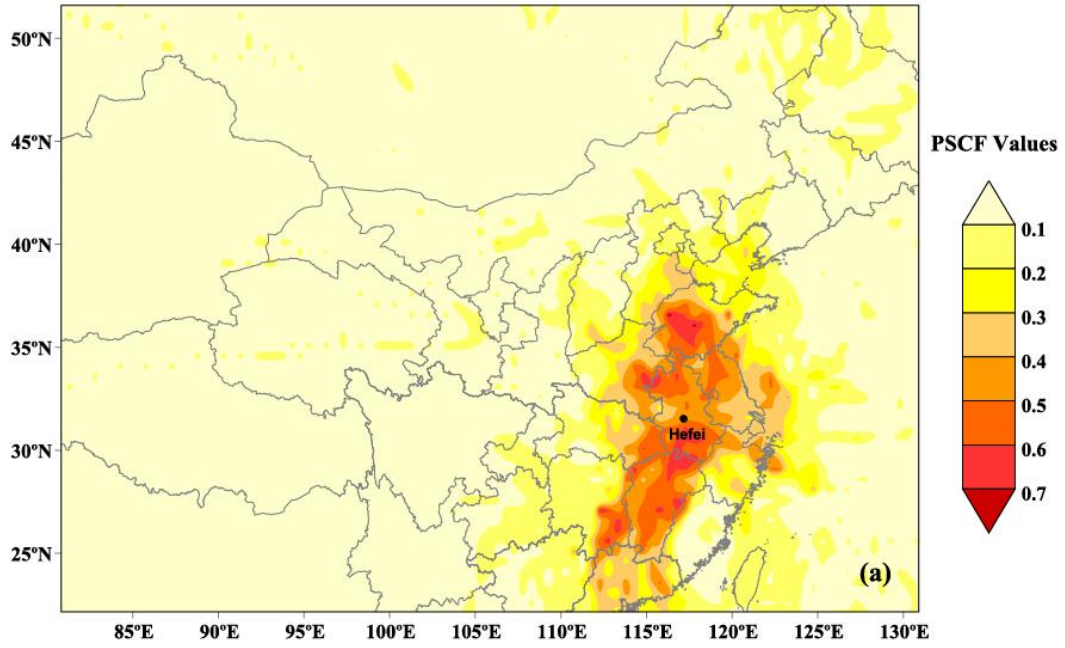
727
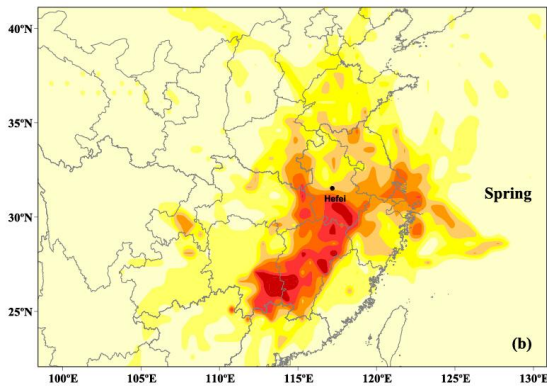
728
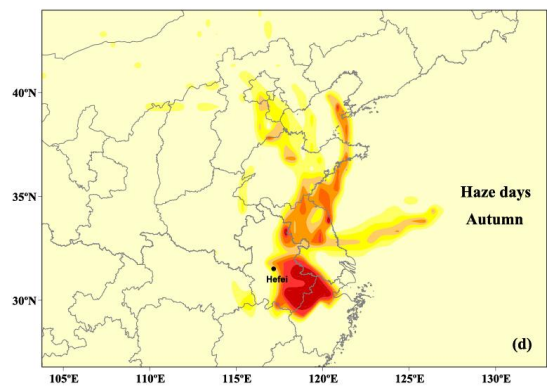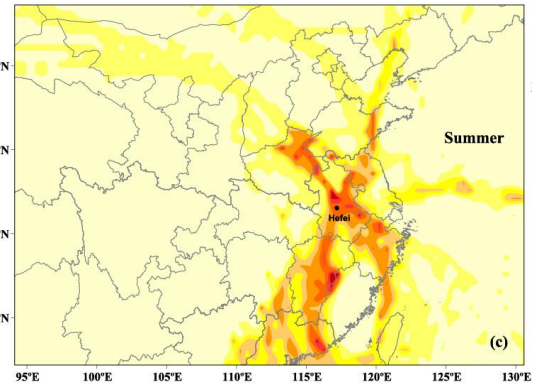
729
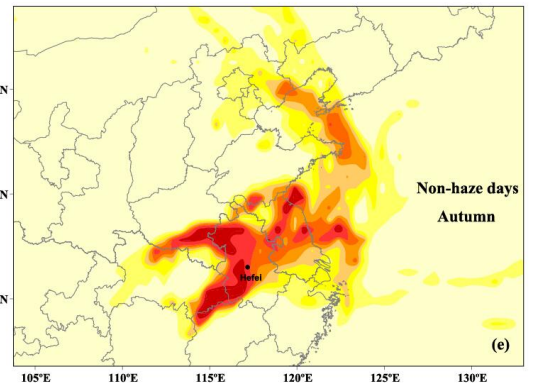
730

731

732

733

734

735
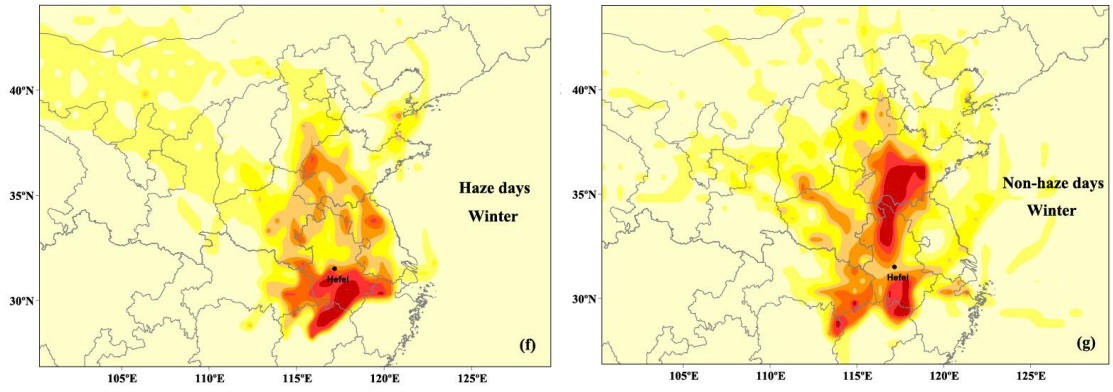
Fig. 4. Likely emission source areas of GEM simulated by PSCF analysis. (a) overall (from July 2013 to June 2014), (b) spring, (c) summer, (d) haze days in autumn, (e) non-haze days in autumn, (f) haze days in winter, (g) non-haze days in winter.

739
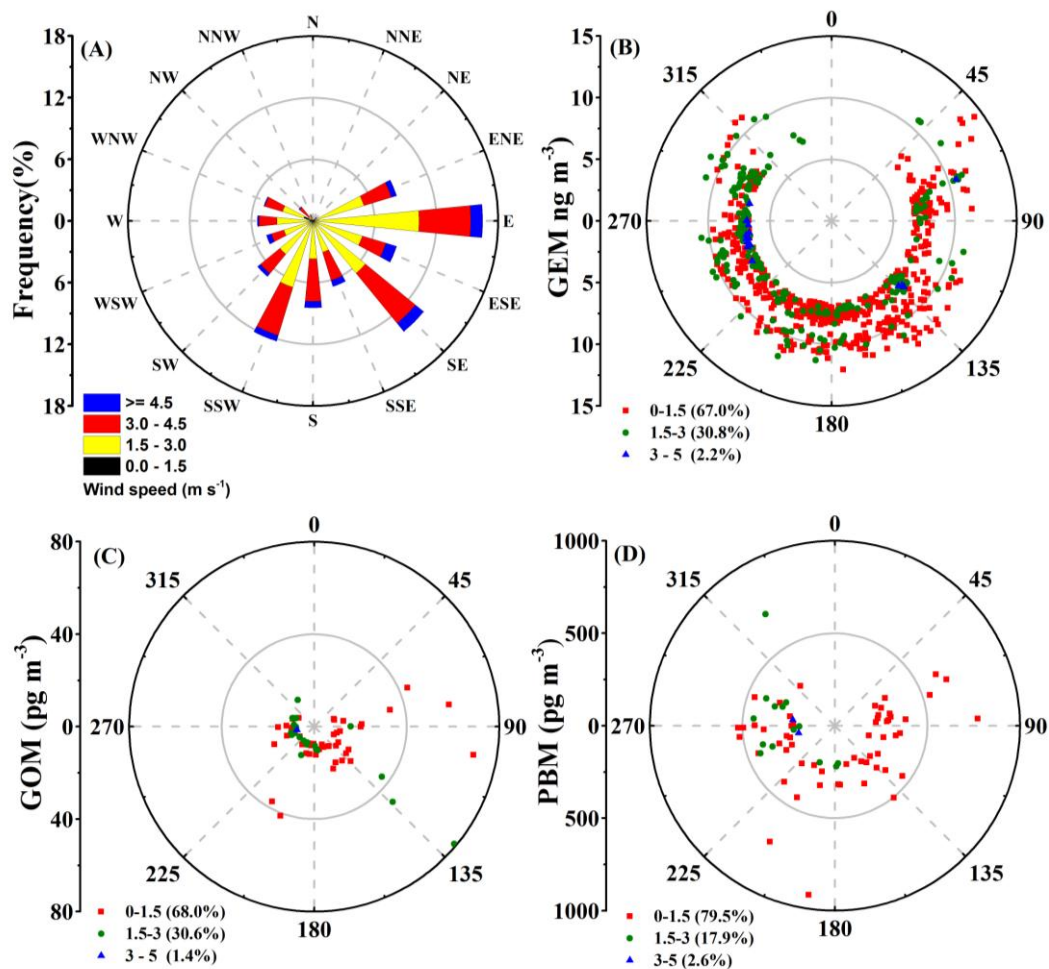
740

741 **Fig. 5.** Wind direction and speed at the Science Island Meteorological Station during

742 the study period. (A) the wind rose for the whole study period; (B), (C) and (D) are

743 the wind rose diagrams for GEM, GOM and PBM concentrations above the 90th

744 percentile values, respectively.

745

746
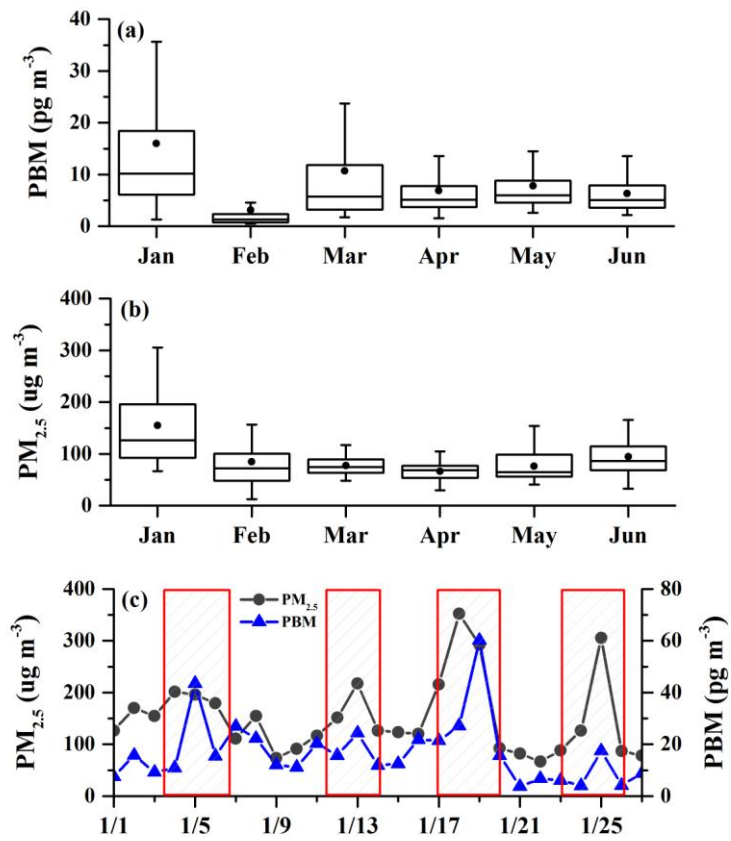
Fig. 6. Monthly variation of (a) PBM and (b) $PM_{2.5}$ concentrations from January to

748   June, 2014, (c) average daily $PM_{2.5}$ and PBM concentrations in January, 2014.

749
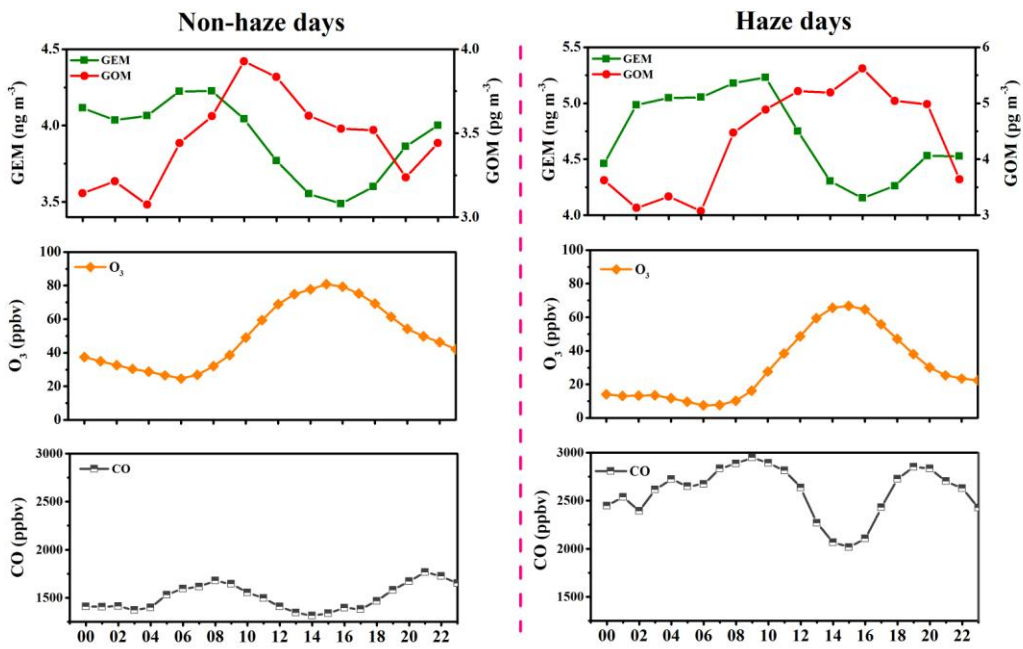
750

751 **Fig. 7.** Diurnal variations of GEM, GOM, O$_3$ and CO concentrations during non-haze

752 and haze days.

753
754
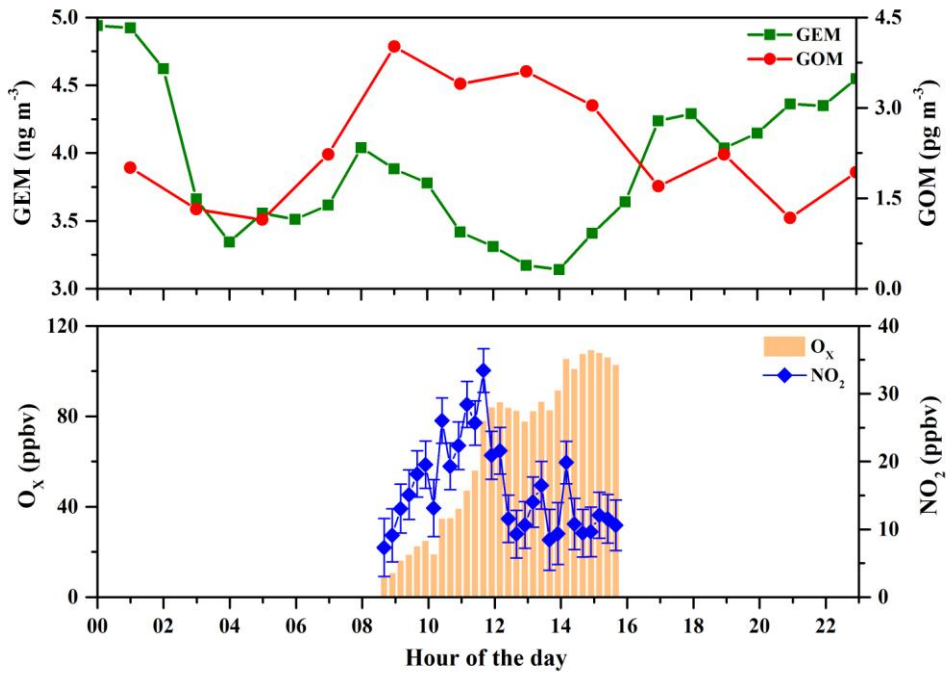
Fig. 8. A case study of diurnal variations of GEM, GOM, O_X, and NO_2 at Hefei (20th November, 2013). The top panel shows the hourly averaged GEM and GOM concentrations, and the bottom panel shows the O_X ($O_X = NO_2 + O_3$) and the NO_2 concentrations. The error bars for NO_2 refer to the NO_2 standard errors.